

## RESEARCH LETTER

10.1029/2018GL077212

## Key Points:

- Moderately strong hiss emissions can occur to peak at  $\sim 100$  Hz within the two crossings of a pronounced post-midnight-to-dawn plume
- Plasmaspheric hiss in the nightside plume is efficient to pitch angle scatter  $\sim 10\text{--}100$  keV electrons
- With the resultant electron loss timescales varying over 3 orders of magnitude, hiss emissions in the nightside plume can account for the fast loss of  $\lesssim 100$  keV electrons and for the slow decay of higher energy electrons

## Correspondence to:

S. Fu and X. Gu,  
fusion@whu.edu.cn;  
guxudong@whu.edu.cn

## Citation:

Zhang, W., Fu, S., Gu, X., Ni, B., Xiang, Z., Summers, D., et al. (2018). Electron scattering by plasmaspheric hiss in a nightside plume. *Geophysical Research Letters*, 45, 4618–4627. <https://doi.org/10.1029/2018GL077212>

Received 21 JAN 2018

Accepted 26 APR 2018

Accepted article online 1 MAY 2018

Published online 22 MAY 2018

## Electron Scattering by Plasmaspheric Hiss in a Nightside Plume

Wenxun Zhang<sup>1</sup> , Song Fu<sup>1</sup> , Xudong Gu<sup>1</sup> , Binbin Ni<sup>1</sup> , Zheng Xiang<sup>1</sup> ,  
Danny Summers<sup>2</sup> , Zhengyang Zou<sup>1</sup> , Xing Cao<sup>1</sup> , Yuequn Lou<sup>1</sup>, and Man Hua<sup>1</sup>

<sup>1</sup>Department of Space Physics, School of Electronic Information, Wuhan University, Wuhan, China, <sup>2</sup>Department of Mathematics and Statistics, Memorial University of Newfoundland, St. John's, Newfoundland, Canada

**Abstract** Plasmaspheric hiss is known to play an important role in radiation belt electron dynamics in high plasma density regions. We present observations of two crossings of a plasmaspheric plume by the Van Allen Probes on 26 December 2012, which occurred unusually at the post-midnight-to-dawn sector between  $L \sim 4\text{--}6$  during a geomagnetically quiet period. This plume exhibited pronounced electron densities higher than those of the average plume level. Moderate hiss emissions accompanied the two plume crossings with the peak power at about 100 Hz. Quantification of quasi-linear bounce-averaged electron scattering rates by hiss in the plume demonstrates that the waves are efficient to pitch angle scatter  $\sim 10\text{--}100$  keV electrons at rates up to  $\sim 10^{-4} \text{ s}^{-1}$  near the loss cone but become gradually insignificant to scatter the higher energy electron population. The resultant timescales of electron loss due to hiss in the nightside plume vary largely with electron kinetic energy over 3 orders of magnitude, that is, from several hours for tens of keV electrons to a few days for hundreds of keV electrons to well above 100 days for  $>1$  MeV electrons. Changing slightly with  $L$ -shell and the multiquartile profile of hiss spectral intensity, these electron loss timescales suggest that hiss emissions in the nightside plume act as a viable candidate for the fast loss of the  $\lesssim 100$  keV electrons and the slow decay of higher energy electrons.

**Plain Language Summary** It is believed that the loss dynamics of radiation belt electrons are coherent with hiss dynamics on spatial scales comparable to the size of the plasmasphere. However, most previous studies focused on the timescale of electron scattering induced by hiss observed in the right plasmasphere. In present work, we first time estimate the electron scattering effect by plasmaspheric hiss in nightside plumes.

### 1. Introduction

Radiation belt electrons can undergo pitch angle scattering through interactions with various wave modes, including whistler mode chorus, plasmaspheric hiss, magnetosonic waves, and electromagnetic ion cyclotron waves (e.g., Cao, Ni, Summers, Bortnik, et al., 2017; Cao, Shprits, et al., 2017; Ni et al., 2013, 2015, 2017; Ni, Cao, et al., 2018; Ni, Zou, et al., 2018; Summers et al., 2007a, 2007b; Thorne, 2010). In particular, as an important physical process in the inner magnetosphere, plasmaspheric hiss is a typically structureless, broadband, and naturally occurring whistler mode emission generally confined within the dense plasmasphere and high-density plasmaspheric plumes (e.g., Carpenter et al., 1993; Chappell, 1974; Laakso et al., 2015; Su et al., 2018; Thorne, 2010), while the fine structure of plasmaspheric hiss has been observed by Van Allen Probes, as recently reported by Summers et al. (2014). It has been long proposed that the formation of the “slot” region between the inner and outer radiation belts is mainly attributed to hiss-induced scattering losses of high energy electrons (Lyons & Thorne, 1973). Furthermore, hiss-induced electron scattering plays a significant role in driving the slow decay of outer zone electrons over a wide range of energies from a few keV to over 1 MeV with the loss timescales varying from about 1 day or less to hundreds of days or more (e.g., Meredith et al., 2006; Ni et al., 2013; Summers et al., 2008; Thorne et al., 2013).

The plasmasphere is a cold (approximately several eV) plasma region of the Earth’s magnetosphere (e.g., Carpenter, 1963; Darrouzet et al., 2009; Goldstein, 2006; Lemaire & Gringauz, 1998). Plasmaspheric plumes are a continuous outward extension of the plasmasphere and may extend far from the Earth, as a result of the interaction between inward moving solar wind-driven convection electric fields and corotational forces after geomagnetically quiet periods (e.g., Goldstein et al., 2014; Moldwin et al., 2004). Plumes preferentially occur during moderate geomagnetic activities at the 14–24 magnetic local time (MLT) interval with the

occurrence rate increasing with the solar wind dynamic pressure (e.g., Darrouzet et al., 2008; Lee et al., 2016; Moldwin et al., 2004). In addition to hiss-induced electron scattering in the plasmasphere, hiss in plumes can also resonate with radiation belt electrons. On the basis of CRRES wave and particle measurements, Summers et al. (2008) investigated in detail 14 representative plumes to consider electron precipitation loss due to pitch angle scattering by hiss in plumes. They found that parallel propagating hiss in plumes can not only directly scatter MeV electrons into the loss cone for atmospheric precipitation but also reduce the generation of MeV electrons by depleting the lower energy electron seed population.

In this study we focus on the observations of two crossings of a plasmaspheric plume by Van Allen Probes on 26 December 2012, which occurred unusually at the post-midnight-to-dawn sector between  $L \sim 4\text{--}6$  during a geomagnetically quiet period and exhibited a pronounced electron density profile much higher than the average plume density level (Moldwin et al., 2004). Moderately strong hiss waves with clear obliquity were captured concurrently by the probes, which thus provides a good opportunity to look into the electron scattering effect by these oblique waves in the quiet time, postmidnight plume. By means of quasi-linear electron diffusion rate computations and loss timescale evaluations, we investigate in detail the role of hiss emissions measured in the observed plume in driving the decay of both radiation belt energetic and relativistic electrons.

The content of the paper is outlined as follows. We illustrate the selected plume crossings and associated hiss wave data in section 2. In section 3, by means of quasi-linear diffusion rate computations and one-dimensional Fokker-Planck diffusion simulations, we investigate in detail the contribution of the measured hiss emissions to resonant scattering of radiation belt energetic electrons and resultant electron loss timescales. We discuss our results and summarize the conclusions in section 4.

## 2. Observations of a Nightside Plume and Hiss Emissions

The twin-satellite Van Allen Probes mission was launched on 30 August 2012 into a geosynchronous transfer orbit, with a perigee of  $1.09 R_E$  ( $1 R_E$  = the radius of the Earth), an apogee of  $5.77 R_E$ , an inclination of  $10.2^\circ$ , and an orbital period of  $\sim 9$  hr (Mauk et al., 2012). For the purpose of this study, we adopt the Level 4 data sets of Van Allen Probes to acquire the ambient plasma density information, which is predominantly extracted from the trace of upper hybrid resonance frequency measured by the High-Frequency Receiver from the Electric and Magnetic Field Instrument Suite and Integrated Science (EMFISIS) onboard the spacecraft (Kletzing et al., 2013; Kurth et al., 2015). The EMFISIS Waveform Receiver (WFR) is used to analyze the wave properties of plasmaspheric hiss.

As a first step of plume determination, we follow the technique of Moldwin et al. (2002) to locate the plasmapause. That is, the plasmapause is identified as the innermost steep gradient in the electron density profile, which requires the electron density to drop by a factor  $>5$  within a half  $L$ -shell. If one Van Allen Probe is outside the plasmapause and if the electron density suddenly increases, remains for a certain period (i.e.,  $>10$  min), and then suddenly decreases, we consider it as a potential plasmaspheric plume. Subsequently, we adopt the rigorous plume selection criteria of Moldwin et al. (2004) for final identification. Specifically, the location of  $L = 3$  is used as a dividing line to decide whether to use the plasmaspheric or trough density model of Sheeley et al. (2001). If the plasmapause is located earthward of  $L = 3$ , a plasmaspheric plume is defined as that whose plasma density exceeds the trough plus one standard deviation density of the Sheeley et al. (2001) model. If the plasmapause is located outside  $L = 3$ , a plasmaspheric plume is defined as that whose plasma density exceeds the Sheeley et al. (2001) plasmaspheric model.

Using the method described above, we capture two obvious plume crossings observed by Van Allen Probe A during a geomagnetically quiet period with the Dst index between 0 and  $-10$  nT on 26 December 2012. The Dst index had a minimum of  $-15$  nT, and the Kp index reached up to 2 during the previous 24 hr. Figure 1a displays the Level 4 density (black curve) data during the period of 12–24 UT. For the purpose of comparisons, the plasmaspheric density (blue curve), plasma trough density (green curve), and twice plasmaspheric density (cyan curve) are also shown following the model of Sheeley et al. (2001). The plasmapause locations are marked by the vertical red curves, on basis of the method of Moldwin et al. (2002), with the outbound one at  $L \sim 3.7$  and the inbound one at  $L \sim 4.0$ . Clearly, there are two pronounced density regions that are outside the plasmapause but well above the twice plasmaspheric density of Sheeley et al. (2001), say, the two crossings of a spatially extended plasmaspheric plume. As shown as shaded regions, one occurred at 1610–1800 UT

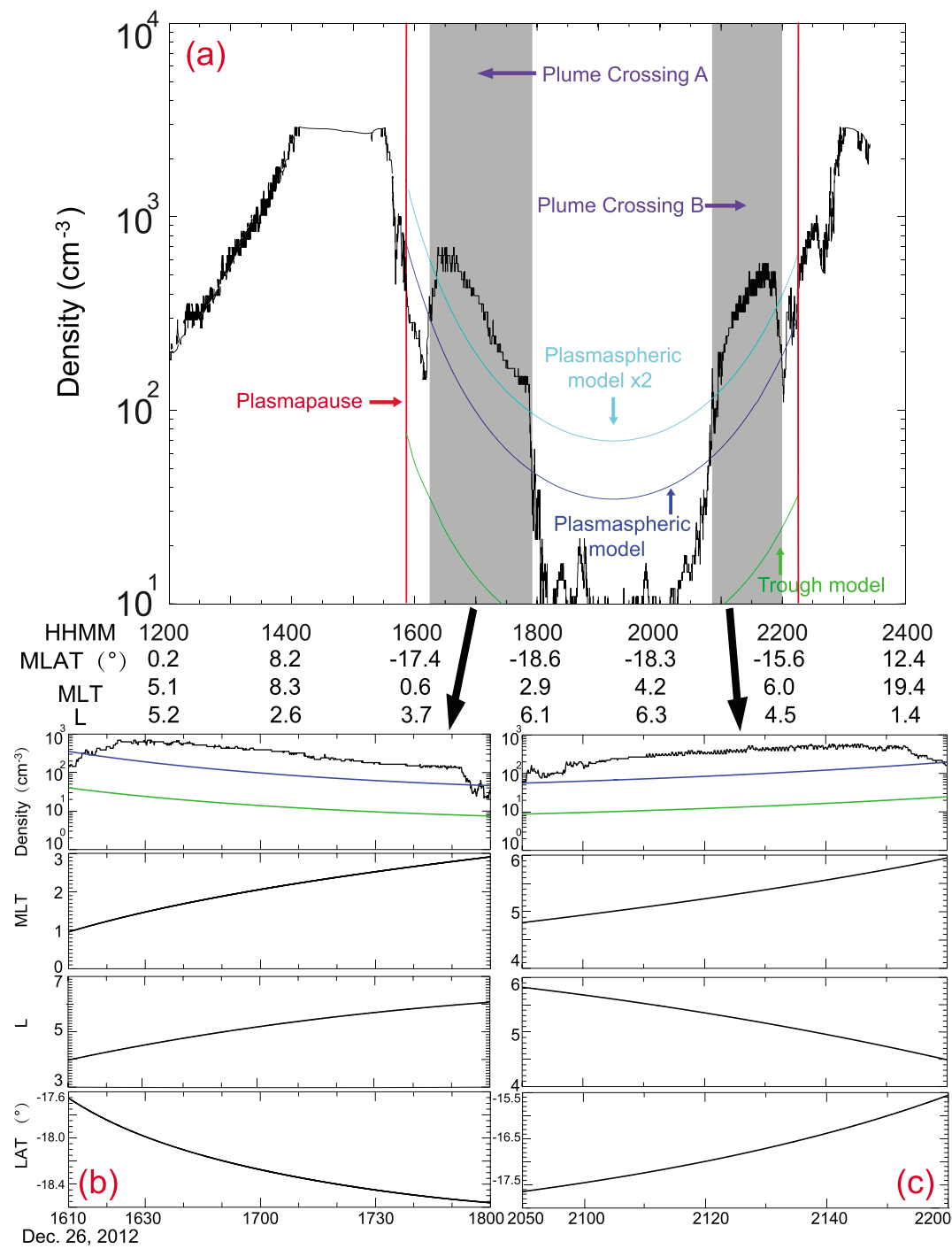


**Figure 1.** (a) Ambient plasma density profile measured by Van Allen Probe A for the chosen plume intervals during 26 December 2012. The blue, green, and cyan curves represent respectively the saturated plasmasphere density, plasma-trough density, and twice plasmasphere density from the model of Sheeley et al. (2001). The vertical red lines denote the plasmapause locations identified following the model of Moldwin et al. (2002). The shaded regions indicate the periods of the selected two plumes (A and B). (b) A zoom-in plot of Plume Crossing A that occurred outbound at  $\sim 01\text{--}03$  MLT,  $L = 4.0\text{--}6.1$ , and  $\text{MLAT} \sim -18^{\circ}$ . (c) Same as in (b) except for Plume Crossing B that occurred outbound at 04:48–06:00 MLT,  $L = 4.5\text{--}5.8$ , and  $\text{MLAT} \sim -16.5^{\circ}$ .

(labeled as Plume Crossing A thereafter) and the other at 2050–2200 UT (labeled as Plume Crossing B thereafter).

Zoom-in plots of these two time intervals are shown in Figures 1b and 1c to provide detailed information of the ambient electron density and the spatial location defined by L-shell, MLT, and magnetic latitude (MLAT) for the plume. Plume Crossing A occurred at 01–03 MLT across  $L = 4.0\text{--}6.1$  with  $\text{MLAT} \sim -18^\circ$  and Plume Crossing B at  $\sim 05\text{--}06$  MLT across  $L = 4.5\text{--}5.8$  with  $\text{MLAT} \sim -16.5^\circ$ . These two plume crossings were on the postmidnight to dawnside, which is rare according to the statistics of plasmaspheric plume (e.g., Darrouzet et al., 2008; Lee et al., 2016; Moldwin et al., 2004). Note that Plume Crossings A and B occurred on the outbound and inbound orbits, respectively. Evaluations of the density profiles observed by Van Allen Probes A and B find that such a plume structure did not occur during the previous and following plasmasphere crossings; that is, the reported plume event is unique for the time period of our consideration.

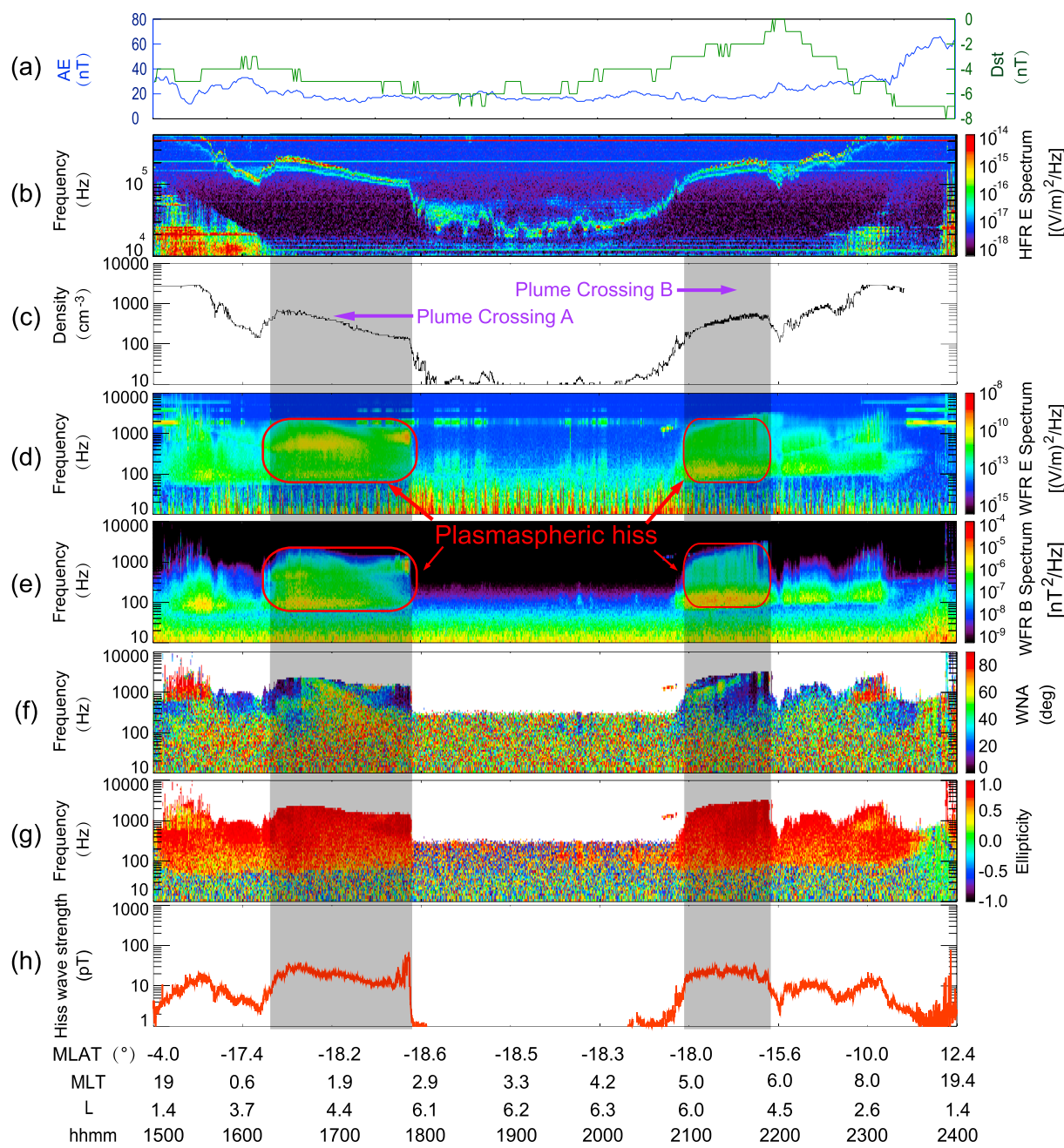
From top to bottom, Figure 2 illustrates the Dst and AE indices, the High-Frequency Receiver electric field spectral intensities, the Level 4 electron density profile, the WFR electric and magnetic field spectral intensities, the corresponding wave normal angle and ellipticity ( $-1$  means left-handed polarization,  $0$  means linear polarization, and  $1$  means right-handed polarization) calculated by the method of singular value decomposition (Santolik et al., 2003) of the WFR emissions, and the integrated hiss wave amplitude profile during the period of 15–24 UT on 26 December 2012. The information of L-shell, MLT, and MLAT is given at the bottom of the figure. The shaded regions indicate the two intervals of Plume Crossing A and Plume Crossing B. It is worthwhile to point out that these two obvious plume crossings occurred under the very quiet geomagnetic activity condition. During the previous 24 hr, Dst had a minimum of  $-15$  nT and Kp reached up to 2, distinct from previous studies (e.g., Darrouzet et al., 2008; Lee et al., 2016; Moldwin et al., 2004). Corresponding to the occurrence of the plume, representative hiss emissions were observed concurrently at frequencies from tens of Hz to  $\sim 2$  kHz. By confining the ellipticity  $>0.8$  for right-hand polarized whistler mode waves, we focus on the hiss frequency range of  $55$  Hz  $< f < 2,000$  Hz in the plume for our following analysis. Within the two plume crossings, the hiss emissions were moderately strong at the similar amplitude level, say,  $\sim 20$  pT (Figure 2h). In addition, the waves occurred at intermediate latitudes with their wave normal angles mainly  $\lesssim 30^\circ$  but occasionally extending to  $\gtrsim 60^\circ$ . Since the plume occurred at intermediate MLATs, the obliquity of the hiss emissions can mainly result from the propagation effect from the source region around the geomagnetic equator to higher latitudes where the curvature and gradient of the ambient magnetic field become significant (Laakso et al., 2015). Hence, the wave obliquity needs to be considered when exploring the wave-particle interactions in the plumes.

In order to evaluate in detail the hiss wave frequency spectrum in the quiet time, postmidnight plume, we select four representative ranges of L-shells for further investigation, that is,  $L = 4.5 \pm 0.1$  and  $L = 5.0 \pm 0.1$  in Plume Crossing A (outbound) and  $L = 5.5 \pm 0.1$  and  $L = 5.0 \pm 0.1$  in Plume Crossing B (inbound). The observations of hiss wave magnetic field spectral intensities are displayed as scatter plots in Figure 3 for the four intervals. In each panel, the wave spectral intensity is plotted every 6 s, and the green, red, blue curves represent the profiles of upper quartile, average, and lower quartile spectral intensity values, which are subsequently adopted for evaluations of hiss-induced electron scattering coefficients. In each panel, we also give the values of the geomagnetic field intensity, ambient plasma density, and hiss wave amplitude that are averaged over the specified narrow L-shell range. For all four considered cases, the average hiss wave spectral intensities peak at  $\sim 100$  Hz, distinct from the frequently adopted “classical” hiss frequency spectrum model with the peak at 550 Hz (e.g., Li et al., 2015; Ni et al., 2013; Summers et al., 2007a, 2007b, 2008). The average hiss wave amplitudes are similar to each other at  $\sim 20$  pT. Note that the two-peak structures of the hiss emissions in Figures 3a and 3b may result from the superposition of two groups of hiss emissions from different sources.

### 3. Hiss-Induced Electron Scattering

#### 3.1. Resonant Scattering Rates

The Full Diffusion Code (Cao, Ni, Summers, Zou, et al., 2017; Ni et al., 2008, 2015; Shprits & Ni, 2009) is used to evaluate the hiss-induced electron scattering rates in the two plume crossings. Contributions from the  $N = -10$  to  $N = 10$  cyclotron harmonic resonances and the Landau resonance  $N = 0$  are included in the computations. The geomagnetic field model is assumed to be dipolar and scaled by the equatorial magnetic field



Dec. 26, 2012

**Figure 2.** (a) Time series of AE and Dst indices, (b) spectrogram of electric field spectral intensity measured by Van Allen Probe A EMFISIS High Frequency Receiver (HFR) with the upper curve representing the trace of upper hybrid resonance frequency ( $f_{\text{uhf}}$ ), (c) the profile of ambient electron density derived from the  $f_{\text{uhf}}$  curve in (b), spectrograms of (d) electric and (e) magnetic field spectral intensity measured by Van Allen Probe A EMFISIS Wide Frequency Receiver (WFR), and the corresponding temporal variation of (f) wave normal angle, (g) ellipticity, and (h) integrated hiss wave strength. The shaded regions indicate the periods of the selected two plumes.

strength obtained from the measurements, which is reasonable for the considered very quiet geomagnetic activity. The ambient plasma density is assumed latitudinally constant, with the values obtained from the measurements as well. Specifically, the ambient electron density is set as  $631 \text{ cm}^{-3}$  at  $L = 4.5$  and  $445 \text{ cm}^{-3}$  at  $L = 5.0$  for Plume Crossing A and as  $491 \text{ cm}^{-3}$  at  $L = 5.0$  and  $285 \text{ cm}^{-3}$  at  $L = 5.5$  for Plume Crossing B. For the waves in the plume, the profiles of average, upper quartile, and lower quartile spectral

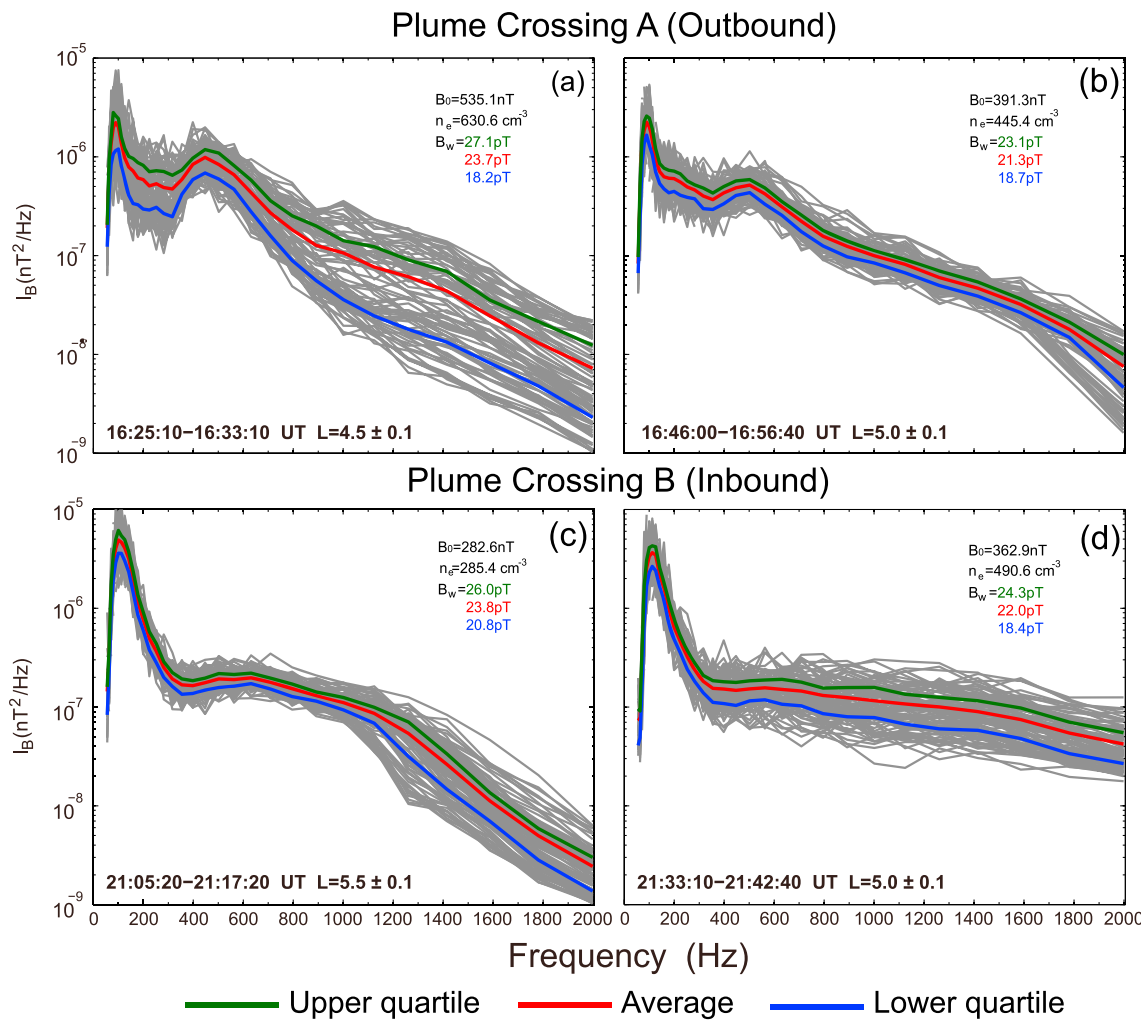


**Figure 3.** Line plot of measured hiss wave spectral intensity as a function of frequency at the indicated L-shells for each of the two chosen plume crossings: (a)  $L = 4.5 \pm 0.1$  and (b)  $L = 5.0 \pm 0.1$  for Plume Crossing A and (c)  $L = 5.5 \pm 0.1$  and (d)  $L = 5.0 \pm 0.1$  for Plume Crossing B. The green, red, and blue curves in each panel represent the profiles of upper quartile, average, and lower quartile spectral intensity values of hiss emissions in the plumes. The color-coded  $B_w$  values correspond to the color-coded multiple quartiles of observed hiss intensities.

intensity in Figure 3, rather than any Gaussian fitting model as were done in previous studies, are used for diffusion rate calculations. The distribution of hiss wave normal angle as a function of latitude is another critical parameter required for numerical computations, which, however, cannot be directly obtained from observations. Therefore, we follow the study of Ni et al. (2013) to adopt the model of hiss wave normal angle distribution as a function of geomagnetic latitude. This model is obtained on the basis of the formation of hiss waves due to the propagation penetration of whistler mode chorus into the plasmasphere (Bortnik et al., 2008, 2009, 2011; Chen et al., 2012).

With all the information above available, we compute the quasi-linear bounce-averaged pitch angle scattering rates  $\langle D_{aa} \rangle$  due to the observed hiss emissions in the two nightside plasmaspheric plume crossings, the results of which are shown as a function of equatorial pitch angle ( $\alpha_{eq}$ ) and electron kinetic energy ( $E_k$ ) in Figures 4a–4l. The first two columns show the results for Plume Crossing A at  $L = 4.5$  and  $5.0$  and the last two columns for Plume Crossing B at  $L = 5.5$  and  $5.0$ . From top to bottom, the results of electron diffusion rates correspond to the adoptions of lower quartile, average, and upper quartile spectral intensity profiles of hiss emissions in the plume.

There are a number of interesting features concerning the profiles of electron pitch angle scattering rates by hiss in the plume: (1) For each considered case, there are two peaks of  $\langle D_{aa} \rangle$  in the  $(E_k, \alpha_{eq})$ -space, both at the

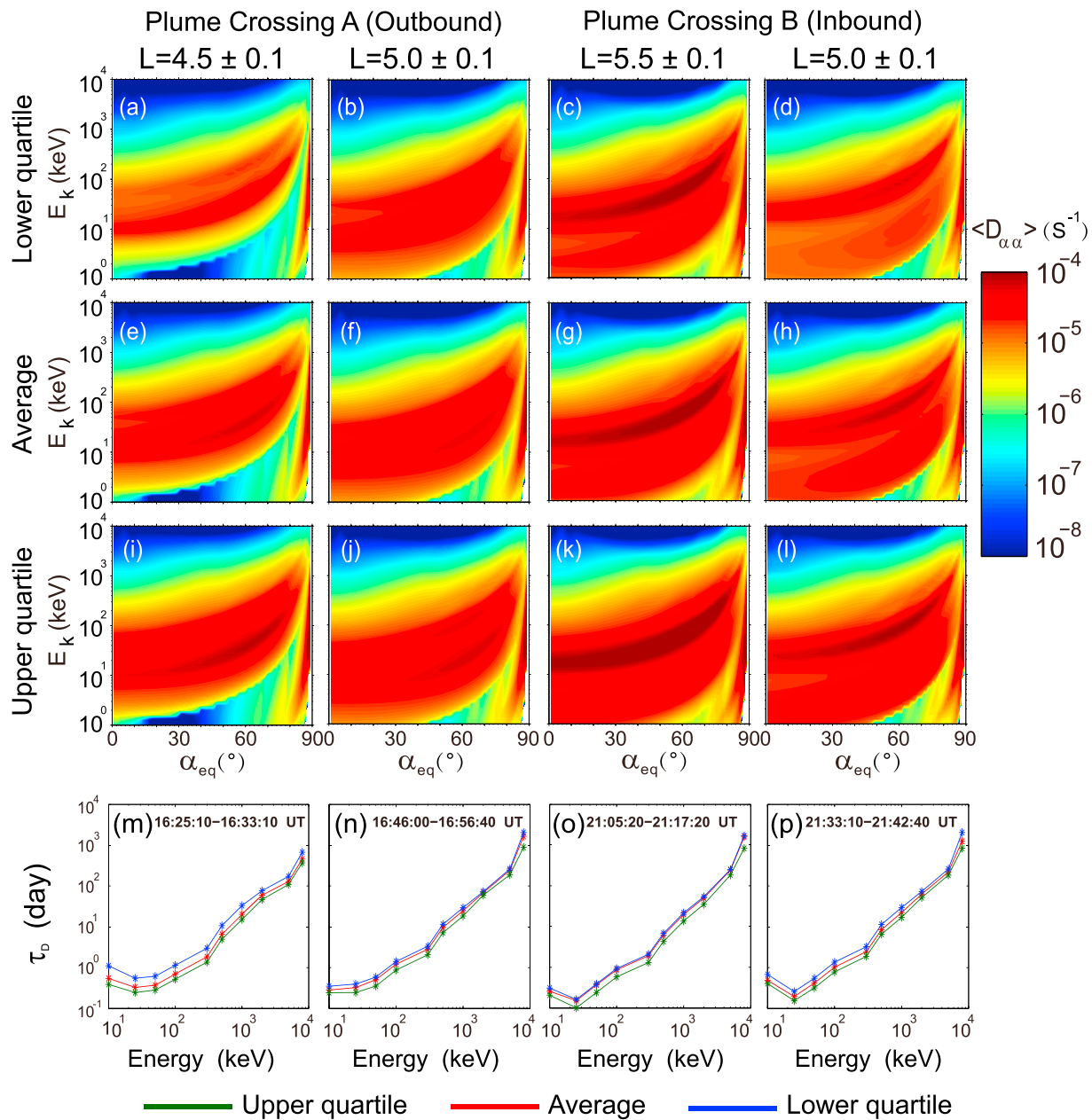


**Figure 4.** Two-dimensional plots of quasi-linear bounce-averaged pitch angle scattering rates as a function of electron kinetic energy and equatorial pitch angle by hiss emissions in the nightside plume at the indicated four L-shells, corresponding to (a–d) the lower quartile, (e–h) the mean average, and (i–l) the upper quartile of measured hiss spectral intensities. The resultant hiss-induced electron loss timescales ( $\tau_D$ ) following the equilibrium state are shown in (m–p) for  $L = 4.5 \pm 0.1$  and  $5.0 \pm 0.1$  in Plume Crossing A and for  $L = 5.5 \pm 0.1$  and  $5.0 \pm 0.1$  in Plume Crossing B.

rates  $\geq 10^{-4} s^{-1}$ . One is located at small and/or intermediate pitch angles and increases with electron kinetic energy (especially at  $\sim 10$ –500 keV), mainly due to the first-order gyroresonant interactions. The other is located very close to  $90^\circ$  pitch angles at energies  $\lesssim 500$  keV as well, owing to the Landau resonance. (2) For both Plume Crossings A and B, the overall diffusion coefficients increase with L-shell, mainly due to the fact that the rates are approximately proportional to the square of the ratio of wave amplitude to ambient magnetic field strength (Summers et al., 2007a). Therefore, the most intense pitch angle scattering coefficients occur at  $L = 5.5$  during the inbound crossing of Plume B, reaching the rates  $> 10^{-4} s^{-1}$  near the loss cone for  $\sim 20$  keV electrons and at  $\sim 85^\circ$  for tens of to hundreds of keV electrons. (3) Comparisons of the hiss scattering rates at  $L = 5.0$  for Plume Crossings A and B indicate that the former peaks at

electron energies lower than the latter and the maximum values of  $\langle D_{aa} \rangle$  are smaller for Plume Crossing A than Plume Crossing B. Since the average hiss wave amplitude and ambient magnetic field intensity and plasma density are very similar to each other for the two L-shells (Figures 3b and 3d), it strongly infers that the differences in wave spectral intensity profile mainly account for the differences in wave scattering rates. (4) Lower quartile, average, and upper quartile spectral intensity profiles of hiss in the plume produce varying values of electron scattering rates. The overall distribution pattern of  $\langle D_{aa} \rangle$  is similar in the  $(E_k, \alpha_{eq})$ -space, but the values are largest for the upper quartile hiss wave profile due to the largest wave power.

### 3.2. Electron Loss Timescales

To further evaluate the scattering loss effect of hiss in the plume on outer radiation belt electrons, we use one-dimensional (1-D) pitch angle diffusion simulations at a fixed L-shell (e.g., Meredith et al., 2009; Ni et al., 2013; Thorne et al., 2013) to model the evolution of electron distribution, by solving the 1-D bounce-averaged Fokker-Planck equation,

$$\frac{\partial f}{\partial t} = \frac{1}{T(\alpha_{eq}) \sin(2\alpha_{eq})} \frac{\partial}{\partial \alpha_{eq}} \left[ T(\alpha_{eq}) \sin(2\alpha_{eq}) \langle D_{aa} \rangle \frac{\partial f}{\partial \alpha_{eq}} \right], \quad (1)$$

where  $f$  is the electron phase space density,  $t$  is the time, and the electron bounce period is approximated as  $T(\alpha_{eq}) = 1.3802 - 0.3198 \left( \sin(\alpha_{eq}) + \sqrt{\sin(\alpha_{eq})} \right)$ , with  $\alpha_{eq}$  as the equatorial pitch angle (Lenchek et al., 1961).

By further assuming that the initial electron phase space density follows a sinusoidal function of equatorial pitch angle, we model the temporal evolution of the energetic electron pitch angle distribution caused by hiss-induced scattering in Plume Crossings A and B. Given electron energy, while the time required to reach the equilibrium state of electron flux distribution varies with pitch angle, the subsequent decay timescales as a whole are pitch angle independent (e.g., Ni et al., 2013). In order to quantify the timescale ( $\tau_D$ ) associated with the exponential decay after the equilibrium state, we follow the method of Ni et al. (2013) to calculate  $\tau_D$  as

$$\tau_D = \frac{t_{n+1} - t_n}{\ln[j_{n+1}(\alpha_{eq})] - \ln[j_n(\alpha_{eq})]}. \quad (2)$$

Here the subscript  $n$  represents an indicator of the simulation time step and is chosen to be much larger than the exponent when the equilibrium is reached. The results for  $\tau_D$  are shown as a function of electron energy for the two plume crossings in Figures 4m–4p, in which the blue, red, and green curves represent the electron loss timescales corresponding to the lower quartile, average, and upper quartile profiles of hiss wave spectral intensity, respectively. Specifically, for  $L = 4.5$  during the outbound crossing of the plume and for  $L = 5.0$  and 5.5 during the inbound crossing of the plume, the diffusion rates peak at tens of keV. In contrast, for  $L = 5.0$  during the outbound crossing, the diffusion rates peak well below 10 keV. There are a number of factors accounting for such differences, including L-shell, background plasma density, and wave spectrum. Corresponding to the diffusion rate profiles for the considered four cases, we can see that the electron decay time minimizes at  $\sim 25$  keV for Figures 4m, 4o, and 4p except for Figure 4n.

Clearly, the resultant timescales of electron loss due to hiss in the nightside plume exhibit large variations with electron kinetic energy over 3 orders of magnitude, that is, from several hours for 10 keV electrons to a few days for hundreds of keV electrons to well above 100 days for  $> 1$  MeV electrons. In contrast, the electron loss timescales show a much smaller trend of decrease with L-shell, mostly within a factor of 5. The multi-quartile variation of hiss wave spectral intensity only introduces slight changes in electron loss timescales within a factor of 2. These results strongly suggest that hiss emissions in the nightside plume, when present, can act as a viable candidate for the fast loss of  $< 100$  keV electrons and for the slow decay of higher energy electrons.

## 4. Conclusions and Discussions

In the present study we have performed a detailed investigation of the electron scattering effect of hiss emissions in two crossings of a nightside plume during a geomagnetically quiet period observed by Van Allen Probes on 26 December 2012. The results of quasi-linear bounce-averaged diffusion coefficient

computations at selected L-shells for each plume are adopted to evaluate the electron loss timescales after the equilibrium state in terms of 1-D Fokker-Planck diffusion simulations. Our major conclusions are summarized as follows:

1. Moderately strong hiss emissions can occur to peak at  $\sim$ 100 Hz within the pronounced post-midnight-to-dawn plume even during a geomagnetically quiet period.
2. Plasmaspheric hiss in the nightside plume are efficient to pitch angle scatter  $\sim$ 10–100 keV electrons at the rates up to  $\sim$ 10–4 s $^{-1}$  near the loss cone but become insignificant to scatter the higher energy electron population.
3. The resultant timescales of electron loss due to hiss in the nightside plume vary largely with energy over 3 orders of magnitude, that is, from several hours for tens of keV electrons to a few days for hundreds of keV electrons to well above 100 days for  $>1$  MeV electrons, but tend to change slightly with L-shell and the multiquartile profile of hiss spectral intensity.

Our analysis results strongly suggest that when hiss emissions are present in the nightside plume, they can feasibly produce the fast loss of  $\lesssim$ 100 keV electrons and the slow decay of higher energy electrons as well. While the hiss waves in Plume Crossings A and B result in the similar effect of electron diffusion, their induced rates of electron scattering tend to be smaller than those produced by the normal hiss emissions in the plasmasphere at L = 3.2 (Ni et al., 2013), which requires further investigation but is left as a future study.

It is worthwhile to note that while we have identified a number of other nightside plumes using Van Allen Probes data sets, such a nightside plume as exhibited in the present study is rare due to its occurrence under a very quiet geomagnetic condition, its particular profile of pronounced plasma density higher than the average plume electron level and its rather long duration with a broad spatial coverage. The two plume crossings (i.e., A and B) actually reflect the broad MLT coverage of one plume observed separately in both inbound and outbound satellite trajectories (e.g., Darrouzet et al., 2006; Goldstein et al., 2014). Our study finds that hiss waves in such plasmaspheric plume have important electron scattering effects complementary to those caused by normal hiss emissions in the plasmasphere. The statistics of plasmaspheric plumes and associated hiss wave properties based on the Van Allen Probes database is one research subject in our following studies.

## Acknowledgments

This work was supported by the NSFC grants 41674163, 41474141, 41204120, 41574160, and 41704162; the Hubei Province Natural Science Excellent Youth Foundation (2016CFA044), and a Discovery Grant of the Natural Sciences and Engineering Research Council of Canada. We thank the Van Allen Probes EMFISIS Science Team including Craig Klezting, William Kurth, and George Hospodarsky for providing the data. The EMFISIS data and Level-4 density data are obtained from <https://emfisis.physics.uiowa.edu/data/index>. The data of geomagnetic indices are available from the NASA OmniWeb (<http://cdaweb.gsfc.nasa.gov>).

## References

- Bortnik, J., Chen, L., Li, W., Thorne, R. M., Meredith, N. P., & Horne, R. B. (2011). Modeling the wave power distribution and characteristics of plasmaspheric hiss. *Journal of Geophysical Research*, 116, A12209. <https://doi.org/10.1029/2011JA016862>
- Bortnik, J., Li, W., Thorne, R. M., Angelopoulos, V., Cully, C., Bonnell, J., et al. (2009). An observation linking the origin of plasmaspheric hiss to discrete chorus emissions. *Science*, 324(5928), 775–778. <https://doi.org/10.1126/science.1171273>
- Bortnik, J., Thorne, R. M., & Meredith, N. P. (2008). The unexpected origin of plasmaspheric hiss from discrete chorus emissions. *Nature*, 452(7183), 62–66. <https://doi.org/10.1038/nature06741>
- Cao, X., Ni, B., Summers, D., Bortnik, J., Tao, X., Shprits, Y. Y., et al. (2017). Bounce resonance scattering of radiation belt electrons by H+ band EMIC waves. *Journal of Geophysical Research: Space Physics*, 122, 1702–1713. <https://doi.org/10.1002/2016JA023607>
- Cao, X., Ni, B., Summers, D., Zou, Z., Fu, S., & Zhang, W. (2017). Bounce resonance scattering of radiation belt electrons by low-frequency hiss: Comparison with cyclotron and Landau resonances. *Geophysical Research Letters*, 44, 9547–9554. <https://doi.org/10.1002/2017GL075104>
- Cao, X., Shprits, Y. Y., Ni, B., & Zhelavskaya, I. (2017). Scattering of ultra-relativistic electrons in the Van Allen radiation belts accounting for hot plasma effects. *Scientific Reports*, 7(1), 17719. <https://doi.org/10.1038/s41598-017-17739-7>
- Carpenter, D. L. (1963). Whistler evidence of a “knee” in the magnetospheric ionization density profile. *Journal of Geophysical Research*, 68, 1675–1682. <https://doi.org/10.1029/JZ068i006p01675>
- Carpenter, D. L., Giles, B. L., Chappell, C. R., Decreau, P. M. E., Anderson, R. R., Persoon, A. M., et al. (1993). Plasmasphere dynamics in the dusk-side bulge region: A new look at an old topic. *Journal of Geophysical Research*, 98, 19,243–19,271. <https://doi.org/10.1029/93JA00922>
- Chappell, C. R. (1974). Detached plasma regions in the magnetosphere. *Journal of Geophysical Research*, 79, 1861–1870. <https://doi.org/10.1029/JA079i013p01861>
- Chen, L., Li, W., Bortnik, J., & Thorne, R. M. (2012). Amplification of whistler mode hiss inside the plasmasphere. *Geophysical Research Letters*, 39, L08111. <https://doi.org/10.1029/2012GL051488>
- Darrouzet, F., De Keyser, J., Décréau, P. M. E., El Lemdani-Mazouz, F., & Vallières, X. (2008). Statistical analysis of plasmaspheric plumes with Cluster/WHISPER observations. *Annales de Géophysique*, 26, 2403–2417. <https://doi.org/10.5194/angeo-26-2403-2008>
- Darrouzet, F., de Keyser, J., Décréau, P. M. E., Gallagher, D. L., Pierrard, V., Lemaire, J. F., et al. (2006). Analysis of plasmaspheric plumes: CLUSTER and IMAGE observations. *Annales de Géophysique*, 24, 1737–1758. <https://doi.org/10.5194/angeo-24-1737-2006>
- Darrouzet, F., De Keyser, J., & Pierrard, V. (Eds.) (2009). *The Earth's plasmasphere: A Cluster and IMAGE perspective* (pp. 55–106). New York: Springer. <https://doi.org/10.1007/978-1-4419-1323-4>
- Goldstein, J. (2006). Plasmasphere response: Tutorial and review of recent imaging results. *Space Science Reviews*, 124(1–4), 203–216. <https://doi.org/10.1007/s11214-006-9105-y>
- Goldstein, J., Thomsen, M. F., & DeJong, A. (2014). In situ signatures of residual plasmaspheric plumes: Observations and simulation. *Journal of Geophysical Research: Space Physics*, 119, 4706–4722. <https://doi.org/10.1002/2014JA019953>
- Kletzing, C. A., Kurth, W. S., Acuna, M., MacDowall, R. J., Torbert, R. B., Averkamp, T., et al. (2013). The Electric and Magnetic Field Instrument Suite and Integrated Science (EMFISIS) on RBSP. *Space Science Reviews*, 179(1–4), 127–181. <https://doi.org/10.1007/s11214-013-9993-6>

- Kurth, W. S., De Pascuale, S., Faden, J. B., Kletzing, C. A., Hospodarsky, G. B., Thaller, S., & Wygant, J. R. (2015). Electron densities inferred from plasma wave spectra obtained by the Waves instrument on Van Allen Probes. *Journal of Geophysical Research: Space Physics*, 120, 904–914. <https://doi.org/10.1002/2014JA020857>
- Laakso, H., Santolik, O., Horne, R., Kolmasová, I., Escoubet, P., Masson, A., & Taylor, M. (2015). Identifying the source region of plasmaspheric hiss. *Geophysical Research Letters*, 42, 3141–3149. <https://doi.org/10.1002/2015GL063755>
- Lee, S. H., Zhang, H., Zong, Q.-G., Otto, A., Rème, H., & Liebert, E. (2016). A statistical study of plasmaspheric plumes and ionospheric outflows observed at the dayside magnetopause. *Journal of Geophysical Research: Space Physics*, 121, 492–506. <https://doi.org/10.1002/2015JA021540>
- Lemaire, J. F., & Gringauz, K. I. (Eds.) (1998). *The Earth's plasmasphere, with contributions from D. L. Carpenter and V. Bassolo* (372 pp.). New York: Cambridge University Press. <https://doi.org/10.1017/CBO9780511600098>
- Lenchek, A., Singer, S., & Wentworth, R. (1961). Geomagnetically trapped electrons from cosmic ray albedo neutrons. *Journal of Geophysical Research*, 66, 4027–4046. <https://doi.org/10.1029/JZ066i012p04027>
- Li, W., Ma, Q., Thorne, R. M., Bortnik, J., Kletzing, C. A., Kurth, W. S., et al. (2015). Statistical properties of plasmaspheric hiss derived from Van Allen Probes data and their effects on radiation belt electron dynamics. *Journal of Geophysical Research: Space Physics*, 120, 3393–3405. <https://doi.org/10.1002/2015JA021048>
- Lyons, L. R., & Thorne, R. M. (1973). Equilibrium structure of radiation belt electrons. *Journal of Geophysical Research*, 78, 2142–2149. <https://doi.org/10.1029/JA078i013p02142>
- Mauk, B. H., Fox, N. J., Kanekal, S. G., Kessel, R. L., Sibeck, D. G., & Ukhorskiy, A. (2012). Science objectives and rationale for the Radiation Belt Storm Probes mission. *Space Science Reviews*, 179(1–4), 3–27. <https://doi.org/10.1007/s11214-012-9908-y>
- Meredith, N. P., Horne, R. B., Glauert, S. A., Baker, D. N., Kanekal, S. G., & Albert, J. M. (2009). Relativistic electron loss timescales in the slot region. *Journal of Geophysical Research*, 114, A03222. <https://doi.org/10.1029/2008JA013889>
- Meredith, N. P., Horne, R. B., Glauert, S. A., Thorne, R. M., Summers, D., Albert, J. M., & Anderson, R. R. (2006). Energetic outer zone electron loss timescales during low geomagnetic activity. *Journal of Geophysical Research*, 111, A05212. <https://doi.org/10.1029/2005JA011516>
- Moldwin, M. B., Downward, L., Rassoul, H. K., Amin, R., & Anderson, R. R. (2002). A new model of the location of the plasmapause: CRRES results. *Journal of Geophysical Research*, 107(A11), 1339. <https://doi.org/10.1029/2001JA009211>
- Moldwin, M. B., Howard, J., Sanny, J., Bocchicchio, J. D., Rassoul, H. K., & Anderson, R. R. (2004). Plasmaspheric plumes: CRRES observations of enhanced density beyond the plasmapause. *Journal of Geophysical Research*, 109, A05202. <https://doi.org/10.1029/2003JA010320>
- Ni, B., Bortnik, J., Thorne, R. M., Ma, Q., & Chen, L. (2013). Resonant scattering and resultant pitch angle evolution of relativistic electrons by plasmaspheric hiss. *Journal of Geophysical Research: Space Physics*, 118, 7740–7751. <https://doi.org/10.1002/2013JA019260>
- Ni, B., Cao, X., Shprits, Y. Y., Summers, D., Gu, X., Fu, S., & Lou, Y. (2018). Hot plasma effects on the cyclotron-resonant pitch-angle scattering rates of radiation belt electrons due to EMIC waves. *Geophysical Research Letters*, 45, 21–30. <https://doi.org/10.1002/2017GL076028>
- Ni, B., Cao, X., Zou, Z., Zhou, C., Gu, X., Bortnik, J., et al. (2015). Resonant scattering of outer zone relativistic electrons by multiband EMIC waves and resultant electron loss time scales. *Journal of Geophysical Research: Space Physics*, 120, 7357–7373. <https://doi.org/10.1002/2015JA021466>
- Ni, B., Hua, M., Zhou, R., Yi, J., & Fu, S. (2017). Competition between outer zone electron scattering by plasmaspheric hiss and magnetosonic waves. *Geophysical Research Letters*, 44, 3465–3474. <https://doi.org/10.1002/2017GL072989>
- Ni, B., Thorne, R. M., Shprits, Y. Y., & Bortnik, J. (2008). Resonant scattering of plasma sheet electrons by whistler-mode chorus: Contribution to diffuse auroral precipitation. *Geophysical Research Letters*, 35, L11106. <https://doi.org/10.1029/2008GL034032>
- Ni, B., Zou, Z., Fu, S., Cao, X., Gu, X., & Xiang, Z. (2018). Resonant scattering of radiation belt electrons by off-equatorial magnetosonic waves. *Geophysical Research Letters*, 45, 1228–1236. <https://doi.org/10.1002/2017GL075788>
- Santolik, O., Parrot, M., & Lefevre, F. (2003). Singular value decomposition methods for wave propagation analysis. *Radio Science*, 38(1), 1010. <https://doi.org/10.1029/2000RS002523>
- Sheeley, B. W., Moldwin, M. B., Rassoul, H. K., & Anderson, R. R. (2001). An empirical plasmasphere and trough density model: CRRES observations. *Journal of Geophysical Research*, 106, 25,631–25,641. <https://doi.org/10.1029/2000JA000286>
- Shprits, Y. Y., & Ni, B. (2009). Dependence of the quasi-linear scattering rates on the wave normal distribution of chorus waves. *Journal of Geophysical Research*, 114, A11205. <https://doi.org/10.1029/2009JA014223>
- Su, Z., Liu, N., Zheng, H., Wang, Y., & Wang, S. (2018). Large amplitude extremely low frequency hiss waves in plasmaspheric plumes. *Geophysical Research Letters*, 45, 565–577. <https://doi.org/10.1002/2017GL076754>
- Summers, D., Ni, B., & Meredith, N. P. (2007a). Timescales for radiation belt electron acceleration and loss due to resonant wave-particle interactions: 1. Theory. *Journal of Geophysical Research*, 112, A04206. <https://doi.org/10.1029/2006JA011801>
- Summers, D., Ni, B., & Meredith, N. P. (2007b). Timescales for radiation belt electron acceleration and loss due to resonant wave-particle interactions: 2. Evaluation for VLF chorus, ELF hiss, and EMIC waves. *Journal of Geophysical Research*, 112, A04207. <https://doi.org/10.1029/2006JA011993>
- Summers, D., Ni, B., Meredith, N. P., Horne, R. B., Thorne, R. M., Moldwin, M. B., & Anderson, R. R. (2008). Electron scattering by whistler-mode ELF hiss in plasmaspheric plumes. *Journal of Geophysical Research*, 113, A04219. <https://doi.org/10.1029/2007JA012678>
- Summers, D., Omura, Y., Nakamura, S., & Kletzing, C. A. (2014). Fine structure of plasmaspheric hiss. *Journal of Geophysical Research: Space Physics*, 119, 9134–9149. <https://doi.org/10.1002/2014JA020437>
- Thorne, R. M. (2010). Radiation belt dynamics: The importance of wave-particle interactions. *Geophysical Research Letters*, 37, L22107. <https://doi.org/10.1029/2010GL044990>
- Thorne, R. M., Li, W., Ni, B., Ma, Q., Bortnik, J., Baker, D. N., et al. (2013). Evolution and slow decay of an unusual narrow ring of relativistic electrons near  $L \sim 3.2$  following the September 2012 magnetic storm. *Geophysical Research Letters*, 40, 3507–3511. <https://doi.org/10.1002/grl.50627>